Turkish Journal of Electrical Engineering & Computer Sciences

http://journals.tubitak.gov.tr/elektrik/

Research Article

Turk J Elec Eng & Comp Sci
(2017) 25: 3381 – 3396

doi:10.3906/elk-1604-348

MRI image enhancement using Biot–Savart law at 3 tesla

Yunus Emre ESİN*, **Ferda Nur ALPASLAN**
Department of Computer Engineering, Middle East Technical University, Ankara, Turkey

Received: 25.04.2016 • **Accepted/Published Online:** 13.01.2017 • **Final Version:** 30.07.2017

Abstract: Coil sensitivity is considered as the most valuable data in the parallel reconstruction of magnetic resonance imaging (MRI). In this study, a novel coil sensitivity map extraction method is introduced for spatially fixed phased array coils. The proposed technique uses the Biot–Savart law with coil internal shape information and low-resolution phase image data to form sensitivity maps. The performance of this method is tested in a parallel image reconstruction task, using the sensitivity-encoding (SENSE) technique. Under the quasi-static assumption and using the duality principle, we computed the sensitivity maps of a phased-array head coil and reconstructed full FOV images. The experiments show that the resulting image quality is higher in terms of sharpness, artifact level, homogeneity, etc. than existing methods that use sensitivity maps calculated only from low-resolution image data. Moreover, several simulations were conducted using an electromagnetic simulation software tool to theoretically prove the success of the proposed technique. Our simulation results indicate that the success of the method depends heavily on the size of the coil elements. A new method for calculation of sensitivity maps is briefly introduced, which increases image quality and homogeneity while reducing the artifacts.

Key words: Magnetic resonance imaging, coil sensitivity profiles, parallel imaging, phased array coils, intensity inhomogeneity correction, sensitivity encoding

1. Introduction

Using the sensitivity of radio-frequency coils for spatial encoding is a widely accepted magnetic resonance imaging (MRI) technique. Several parallel imaging techniques [1], such as sensitivity encoding (SENSE) [2] and GRAPPA [3], are commercially available for clinical use. The magnetic resonance images can be reconstructed with a significantly reduced data set, using the spatial variation information in the sensitivity of the elements of each coil. As stated in [4], in a parallel MRI, one of the most important steps is the measurement of coil sensitivity. In typical implementations, either the low-resolution data are collected as part of the prescan, or the examination is performed by collecting additional k-space lines to estimate coil sensitivity [5].

If the coil shape or position is not fixed, methods using additional lines have advantages over those using prescan information, because they are not affected by coil position or shape changes between each scan. When the coil shape and position are fixed, sensitivity data collection can be carried out during prescan to increase efficiency, since this calibration step is carried out once at the beginning of the examination, and is used in all scans during the remaining image acquisition process. However, if the subject moves in the subsequent scans, the sensitivity map found in the prescan step may not be geometrically aligned with the subject, thus causing additional artifacts. In all these approaches, the sensitivities are computed using low-resolution data, which

*Correspondence: esinyunusemre@gmail.com

may affect the quality of the reconstructed images. For example, the reconstruction process may eliminate the fine details that are vital for the diagnosis or treatment of an illness. Further advantages and disadvantages of these methods have been reviewed in [5].

In this study, we use a commercial head coil (Siemens 32ch Head Coil), which is fixed to the patient table and is rigid (i.e. its shape does not change). Currently, head scans constitute a significant percentage of MRI examinations, and most available head coils are rigid and attached to the table. According to [6], MRI provides more comprehensive information for the head and nerve systems than any other medical imaging technique. MRI is the most sensitive scanning test of the head in clinical practices. Therefore, any improvement in the quality of head MR images and scans will have significant impact on clinical practices.

In a recent study, coil sensitivity maps were found by using both the body coil and the phased array coils during the prescan [2]. The image acquired from each element of an array coil is divided by the uniform images from the body coil to determine the corresponding sensitivity map. The map can be used in parallel imaging algorithms as well as in solving coil inhomogeneity problems [7]. Although the birdcage body coil images are fairly uniform, this assumption is not always valid, and becomes more problematic as the main field strength increases. In addition, the noise and artifacts on these images may cause a significant error in the sensitivity maps, especially around the regions where signal intensity is weak. In another study [8], the advantages and disadvantages of autocalibration methods, which acquire sensitivity information immediately before, during, or after the scan, were discussed, and it was shown that as the coil elements become smaller, it is more challenging to obtain an accurate sensitivity map. An alternative option is obtaining extra reference lines in each scan to estimate the coil sensitivities. However, this increases the scan time considerably, which contradicts the main objective of parallel imaging. Moreover, since the reference lines provide low-resolution images, they are susceptible to the Gibbs phenomenon [9]. The fine details in the reconstructed images may also be lost due to low resolution.

We propose a novel method to build coil sensitivity maps. In this method, the magnitude information of sensitivity maps is calculated, and, thus, coil sensitivities are not affected by the artifacts caused by wrong magnitude estimations, such as the Gibbs phenomenon, patient movement, and receiver inhomogeneities. Moreover, compared to the well-known sensitivity estimation methods (i.e. the sensitivity maps found in low resolution reference images), the proposed method forms higher resolution sensitivity maps, which results in more enhanced reconstructed images.

2. Theory

Coil sensitivities can be calculated using the reciprocity principle [10]. It was shown that the spatial distribution of the circularly polarized component of the magnetic field, B_1^- generated by the coil element when a unit current is applied to the terminal of the coil, is proportional to the sensitivity distribution of this coil element. In this study, we assume that the size of the coil is small (with a diameter of less than 10 cm), it has a simple loop structure (not necessarily circular), and the current applied to the terminal of the coil remains unchanged on the wire of the coil.

According to [11], the reciprocal fields can be calculated using Biot–Savart integration when the object size is smaller than the RF wavelength. If this condition is preserved, the geometry of the RF field is hardly affected by the presence of the scanned object. In this study, our target object is the human head. Typical human head sizes are listed in [12]. As stated in [13], average RF wavelength for in vivo brain imaging is 27 cm at 3 T, which is greater than typical human head sizes. In addition, the sensitivity area of a coil depends on its

size, and its sensitivity decreases rapidly with increasing distance from the coil [14]. The region where each coil channel retrieves high signal is known to be smaller than a typical head size. Therefore, in phased array coils, each channel is arranged properly to achieve maximum image quality. Magnetic field at a position of interest due to a current in a wire can be calculated using the Biot–Savart law under quasi-static assumption, as the magnetic field contribution of a unit current on an infinitesimal wire segment, $\vec{dl}$, at position $\vec{r}$ with respect to the point of interest [15]. According to [16], this assumption is valid if the receiver coils are much smaller than the wavelength at the Larmor frequency. The RF field wavelength outside the body is 234 cm, and inside the body it is approximately 30 cm at 3 T [17]. All this information validates our assumptions for such a study, since our head coil element diameters are about 8 cm for all channels. Then we can calculate the magnetic field as

$$d\vec{B} = \frac{\mu_0}{4\pi|\vec{r}|^3}\vec{dl} \times \vec{r},$$

where μ_0 is the constant representing the permeability of free space.

3. Method

The main aim of this study is to discover the spatial coil sensitivity maps using the geometry of the array elements. The proposed method has two steps: sensitivity map derivation and parallel image reconstruction.

3.1. Sensitivity map derivation

The sensitivity magnitude of the coil element at a position in the space is directly proportional to the magnetic field strength at that location, when there is a unit current in its wire loop, provided that the imaged object size is smaller than the RF wavelength at the Larmor frequency. If this condition is satisfied, according to [11], the magnitude of the magnetic field variations due to load (body) can be ignored for coil elements with a diameter smaller than the RF wavelength. In addition, the coil tuning is assumed to be nearly optimal, which is satisfied in our coil. Coil sensitivity maps are complex-valued data that can be represented in terms of magnitude and phase information. In this study, we find the magnitude and phase of the sensitivity map values separately, and then combine them to form the complex-valued final maps. The formula of a typical sensitivity map (S) derivation using magnitude (M) and phase (P) is $S = M \times e^{jP}$.

The 3D sensitivity maps of each channel in a multichannel coil can be computed using the Biot–Savart law. The shape of the wires in each channel can be defined as a combination of several finite straight wires. We calculate the magnetic field (B) using

$$B = \frac{\mu_0 I}{4\pi R}[cos(\alpha) + cos(\beta)]$$

In the equation, μ_0 represents permeability of the free space, which is approximately the same as the human body. Figure 1 illustrates the magnetic field at a position P, due to a current I in a straight finite wire. Distance R and angles α and β can be seen in the figure. The x and y components of the magnetic field for each current segment can be calculated using the geometrical position of the wire segment and the right hand rule. Using this information, the complex value B_1^- can be calculated as the sensitivity of the coil as the sum of all current segments. Then the complex numbers are converted to absolute values to find the magnitude information. Additionally, for each voxel inside the imaging plane, a sensitivity value is calculated for each element of the coil. A sample coil element is shown in Figure 2 as an octagonal wire.

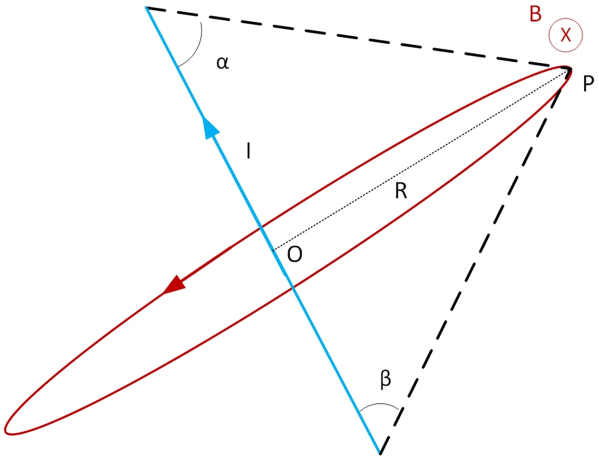

Figure 1. Magnetic field generated at point P by current I in a finite straight wire (shown in blue). Magnetic field on the red circle is constant and tangential to it.

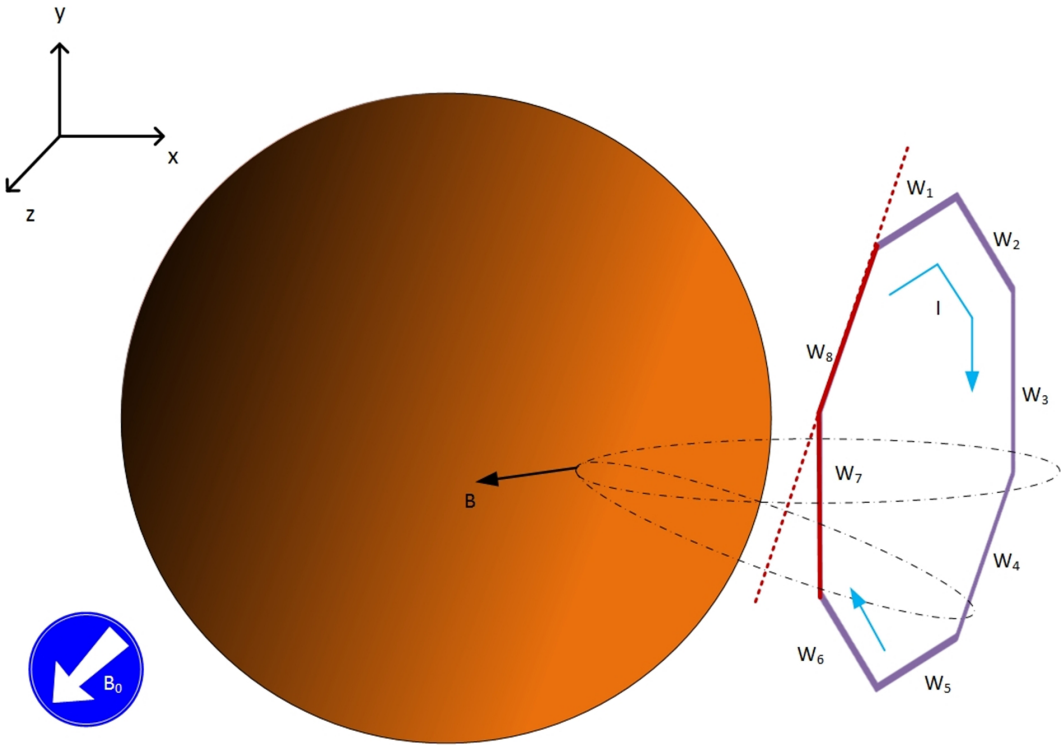

Figure 2. Magnetic field at position P due to a current I in a wire loop is the vector sum of the magnetic field due to each wire segment. The sphere represents the object to be imaged.

A Siemens 3T MRI scanner was used in the experiment. To demonstrate the performance of the new method, we obtained images in normal (without acceleration) and in SENSE (commercial name is mSENSE [18] in our scanner) modes. Moreover, a 32-channel head coil was used in the experiments, which had outer dimensions of 300 mm $\times$ 309 mm $\times$ 290 mm and an internal diameter size of about 22 cm. Each coil element has a diameter of less than 10 cm. According to the head sizes given in [12], a minimum distance of 1–4 cm is expected between the head and each coil element.

Scan data contain table location and corresponding slice position information. All these values are given in the machine's coordinate system. Therefore, image position with respect to head coil location was found, and the positions of the coil wire loops were calculated for each image. We obtained the sensitivity values for a volume of coil size (where the head was located) and with a resolution of 1 mm $\times$ 1 mm $\times$ 1 mm voxel size. (A better resolution can be calculated.) Thus, the spatial coil sensitivity magnitude data of the head are obtained for each channel. Moreover, we prepared a 3D model of the head coil and rendered it in OpenGL in order to visualize the coil elements, scan data, and calculated maps. Figure 3 presents a snapshot of the program.

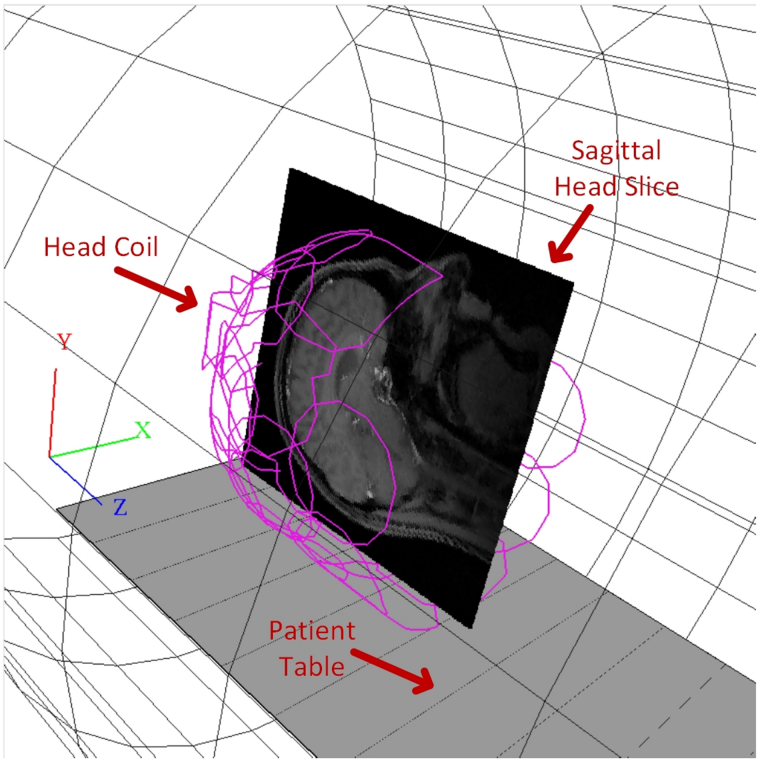

Figure 3. 3D modeling of the 32-channel head coil used in the study, a sagittal head slice image, and the patient table of the MR machine. Grids show the magnet bore of the machine.

Phase information for sensitivity maps is retrieved from the raw scan data files. They are obtained from the scanner and contain MR signal data with scan configuration information. In mSENSE mode, our MRI machine creates two different complex-type data for each channel. One is the fully sampled central region of k-space data, and the other is the undersampled k-space data. In this study, we used the former data to construct the phase data of our sensitivity maps by applying, firstly, the Fourier transform, and then taking $tan^{-1}(Imag/Real)$ of the complex data. We also applied the Fourier transform to undersampled data and obtained the aliased images.

3.2. Parallel image reconstruction

We used the SENSE technique for parallel image reconstruction. Even though the machine uses mSENSE and is significantly different to ours in terms of sensitivity map derivation, both are similar in their usage of sensitivities to form final images. With these methods, final images are constructed by solving a set of linear equations with an unknown number, which is equal to the acceleration factor that defines the gap between each

adjacent line in k-space. For an acceleration factor α in a 2D image, after acquisition of one k-space line, the next $\alpha - 1$ lines are skipped in phase-encoding direction in full k-space. Thus, as the gap between the actual lines is increased, the total lines in the k-space and total scan time are decreased. After the sensitivities of the coil channels are determined and aliased images are formed, the last step is to construct the final image using the SENSE method. This technique aims to unfold the aliased images using the sensitivities of the coil channels, as explained in [19].

4. Experiments and results

We carried out several experiments on both real MRI scan data and simulation data.

4.1. Experiments on real scan data

The proposed method is tested with different scan configurations on a spherical phantom and seven volunteers with different head sizes. The tests were performed on several MR images with various slice orientations and positions. The experiments were conducted with the approval of the Human Subject Ethics Committee, Middle East Technical University. Coil sensitivities were calculated using the proposed method. The magnitude and phase image maps are shown separately in this section.

Figure 4 is an illustration of the calculated sensitivity magnitude map of an element of the 32-channel head coil. In this figure, a coil element and its location, corresponding to the slice position, is shown in a 3D model (Figure 4a). Moreover, the calculated sensitivity map and the channel's raw image are also shown. Figure 5 shows the phase image generation process from low-resolution scan data corresponding to another coil element. When Figures 5a and 5b are compared, the magnitude image is more affected by the object shape and internals (such as different types of tissues) than the phase image. Although the signal intensities are very low in some regions of the imaging object, the phase information can still be extracted from these regions. This is the main reason why we use the phase image and calculate the magnitude image using the proposed method. Moreover, although the calculated sensitivity map is smooth, the found map is adversely affected by the object internals, noise, and low resolution.

The images in Figures 6a and 7a show SoS of absolute signal data from 32 channels. They are obtained from a volunteer and a phantom. The images in Figures 6b and 7b show the SoS obtained with the manufacturer's reconstruction technique. The images in Figures 6c and 7c show the output of the proposed method. The images obtained using the manufacturer's software and the proposed method can be compared under different conditions. For a detailed analysis, the magnified and color map mode versions are provided in panels (d) and (e) of Figures 6 and 7. Artifacts are shown with red arrows in the corresponding magnified images. The errors in the reconstructed images can be detected in the regions where no signal is expected (i.e. outside the scanned objects). As can be seen, the proposed reconstruction has fewer artifacts outside the head and phantom images, indicating that the sensitivity map, calculated using the proposed formulation, is more accurate than the map found using acquired MR data. In addition, Figure 8 gives the performance of our method on intensity correction.

4.2. Experiments on simulation data

In addition to the scan data, we used a commercial electromagnetic simulation software tool (FEKO) to simulate the B_1^- magnitude changes over a phantom, depending on the coil size and distance between the coil and a phantom load at 3 T. We prepared three different-sized square coils with a side length of 6, 9, and 12

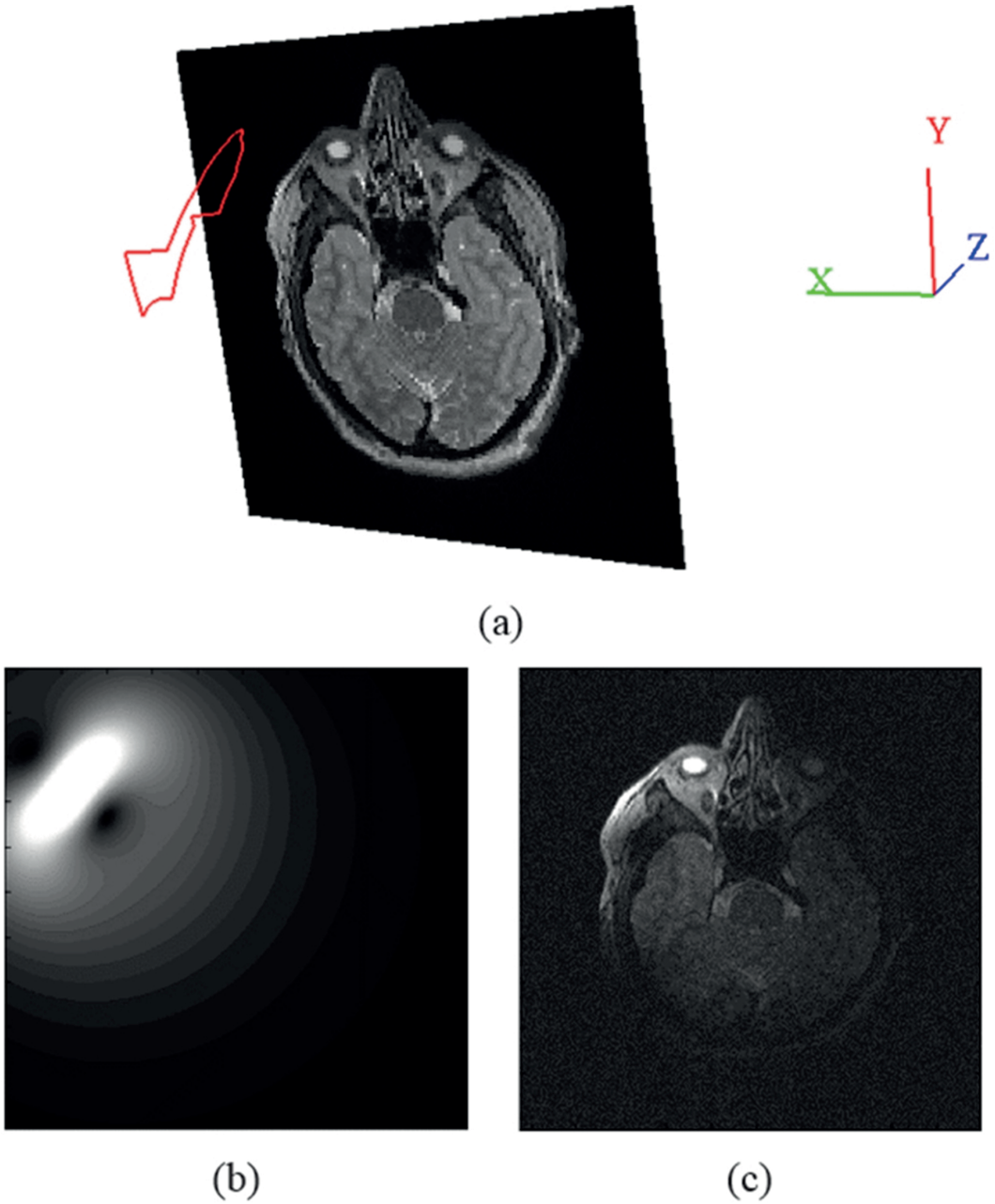

Figure 4. Sensitivity map calculated from an element of the 32-channel head coil: (a) 3D model of a channel and image slice position; (b) sensitivity map; (c) image obtained using only this element of the coil.

cm, respectively, and a phantom with a relative permittivity of 61.0 and conductivity (S/m) of 0.22. In the experiments, coils are positioned at a distance of 1, 3, 5, and 7 cm to the phantom, and for each B_1^- magnitude, values are collected with a resolution of 0.5 cm over a line starting from the coil center and going through the phantom center. The magnitudes are normalized according to the point where the phantom begins. Figure 9 shows a screen shot of an experimental setup and the results of each experiment.

In this study, we used the principle of reciprocity and assumed a steady current flowing in the coil element. In order to validate this approach, as well as the magnitude changes, we also analyzed the current variations

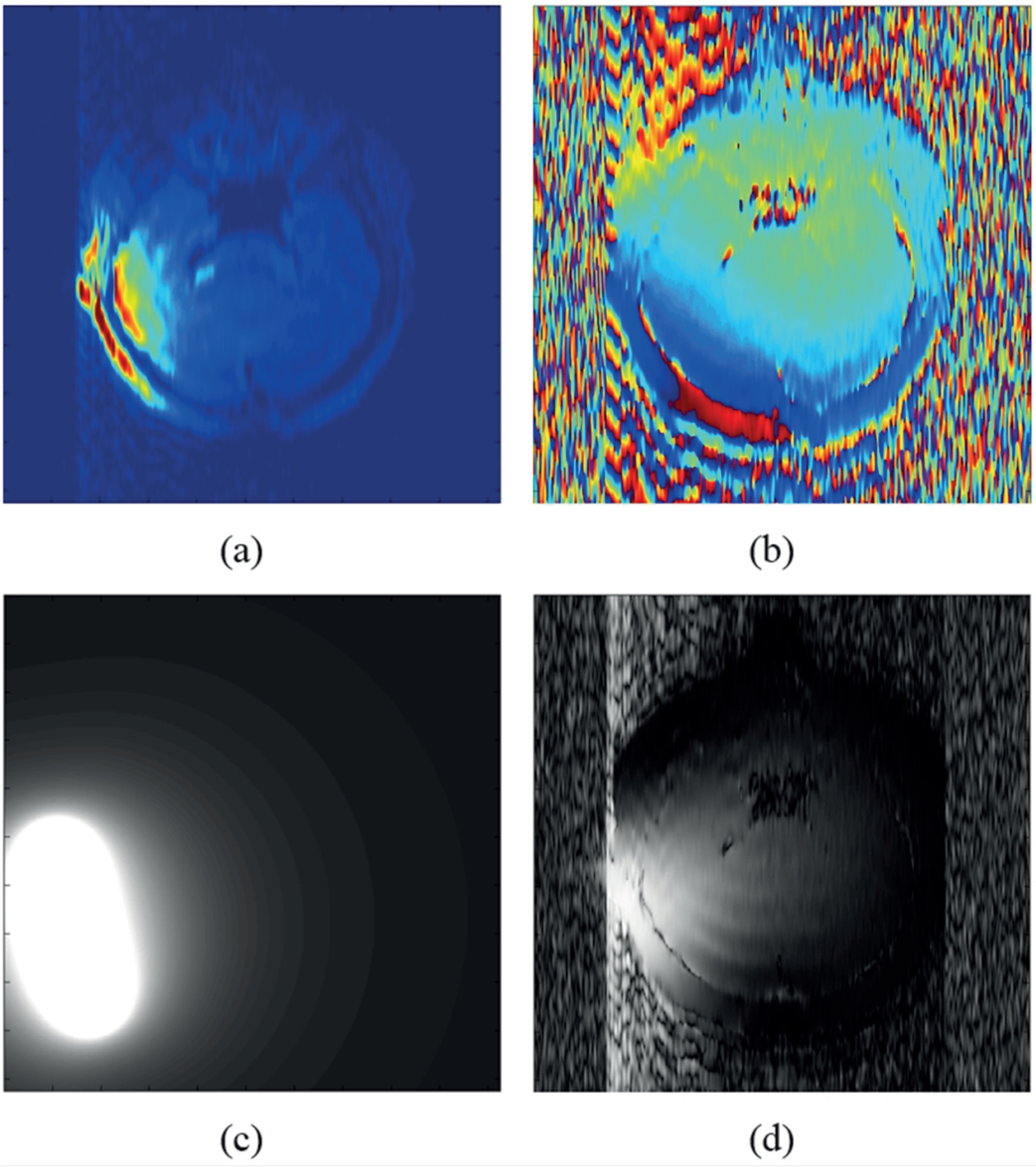

Figure 5. Sensitivity map calculation of a coil channel element: (a) Magnitude image of the channel constructed from reference low-resolution data; (b) phase image of the channel; (c) magnitude image calculated from the Biot–Savart law; (d) sensitivity map magnitude image, calculated by dividing the image in (a) with SoS of all channels' low-resolution magnitude images.

over the coil element. The percentage of the differences between the two ends of the coil conductor is provided in the Table. Current change is less than 1% in all cases. Moreover, the current difference is maximum when the distance between the coil and the phantom is 1 cm. Depending on the coil size and coil-to-phantom distance, even smaller current variations were obtained.

5. Discussion

In this study, several experiments were carried out and different aspects of the proposed method were analyzed on both real-world and simulation data. According to the experiments on real scan data, the results of the proposed

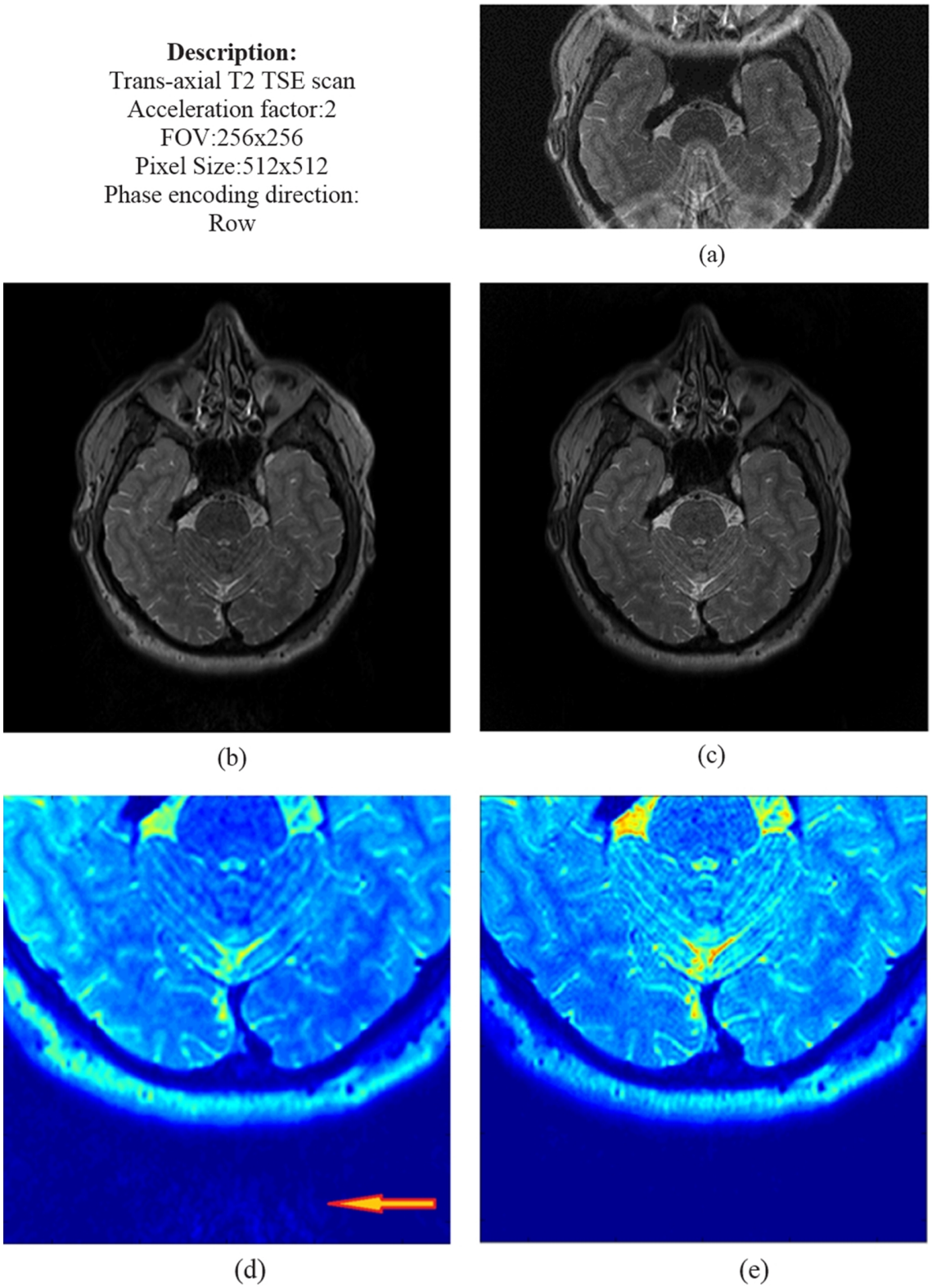

Figure 6. Transaxial T2 TSE head scan experiment image data: (a) SoS of absolute signal data from 32 channels; (b) MRI scanner output using the mSENSE method; (c) result of the SENSE method using a calculated sensitivity map; (d) magnified bottom part of image given in (b), with artifacts marked with red arrows; (e) magnified bottom part of image given in (c).

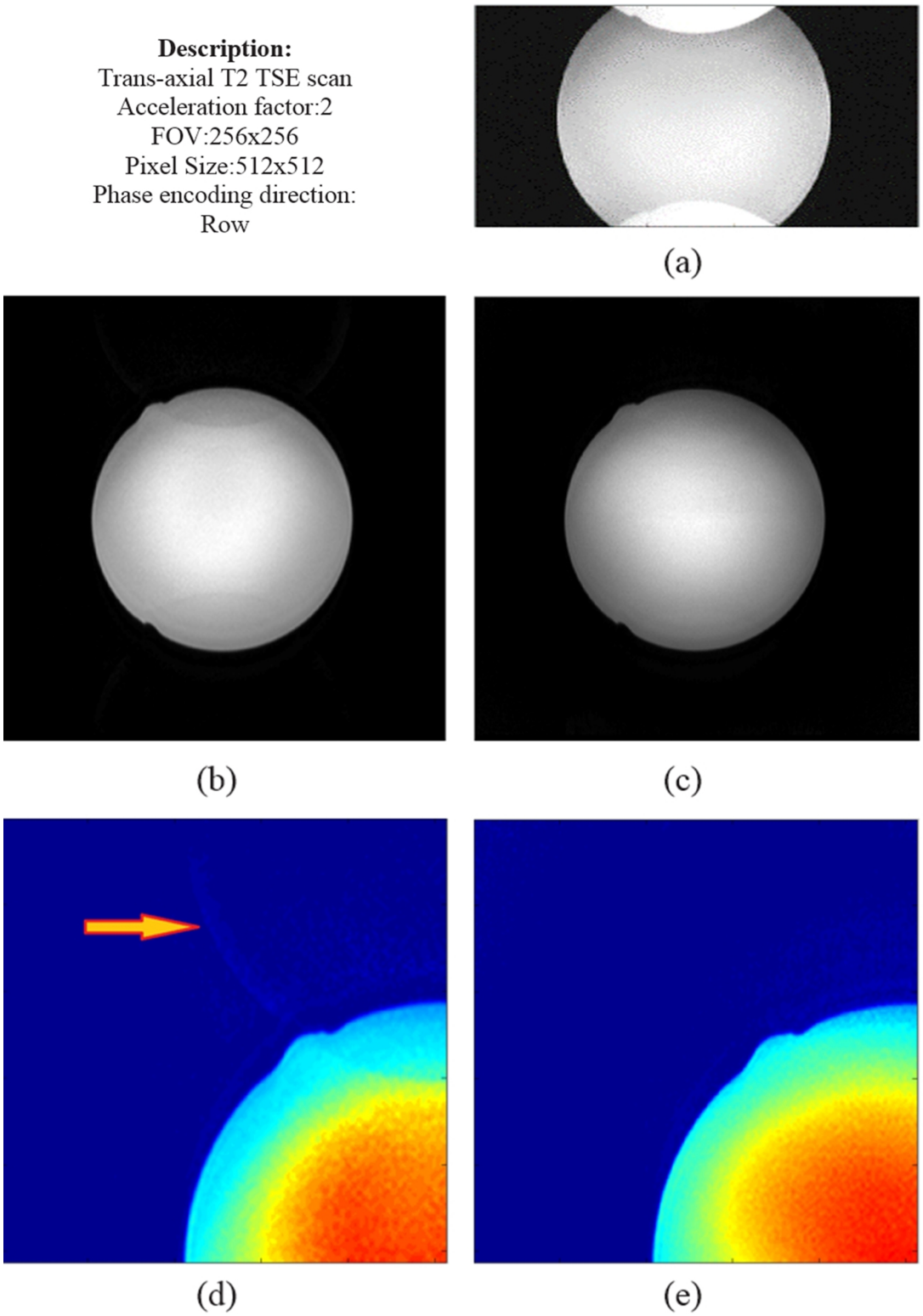

Figure 7. Transaxial T2 TSE phantom scan experiment image data: (a) SoS of absolute signal data from 32 channels; (b) MRI scanner output using the mSENSE method; (c) result of the SENSE method that uses calculated sensitivity map; (d) magnified bottom part of image given in (b) and artifacts are marked with red arrows; (e) magnified bottom part of image given in (c).

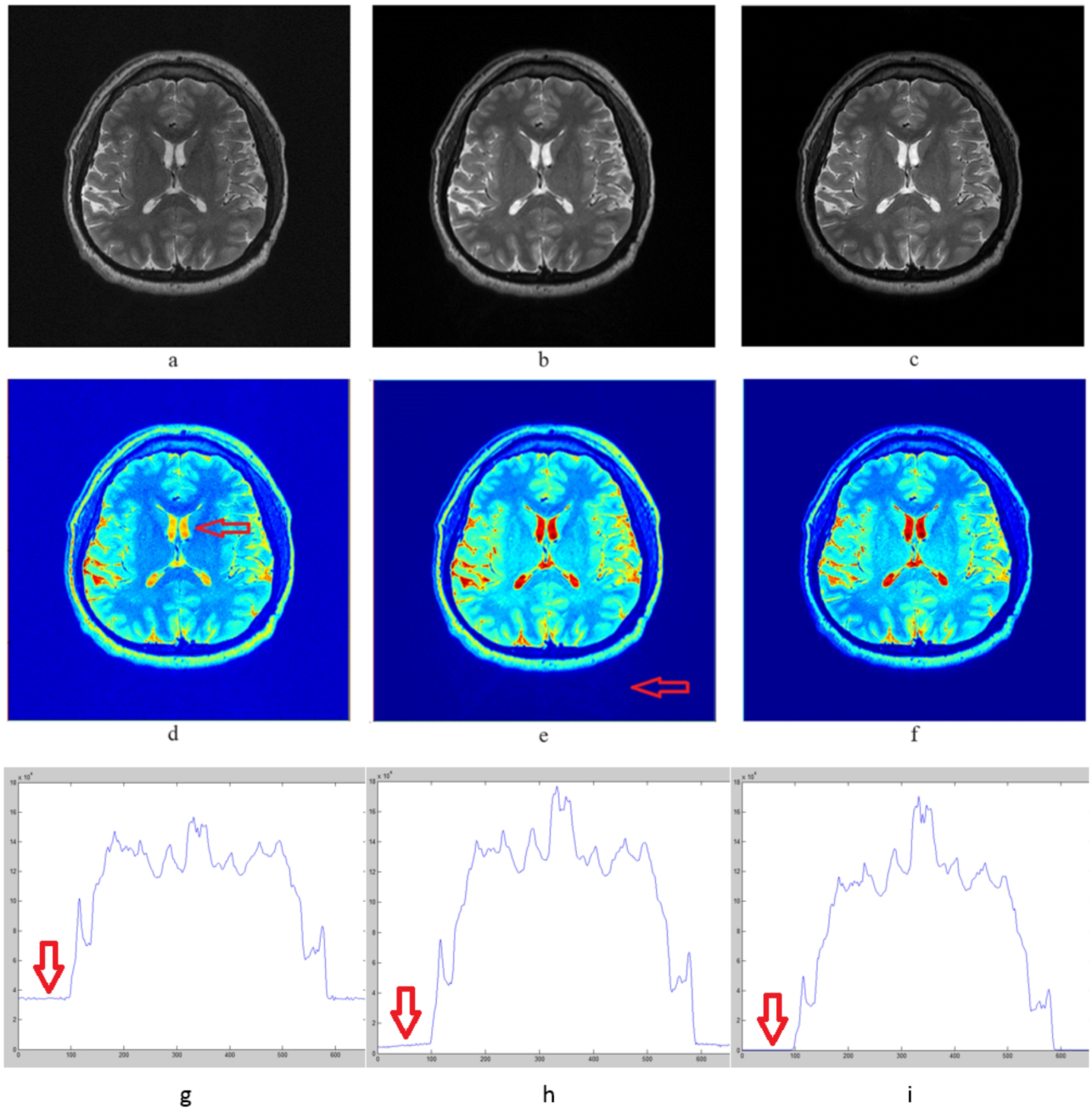

Figure 8. Combination of each channel's signal data: (a) SoS of absolute signal data from 32 channels; (b) MRI machine output image; (c) provided methods combination. In SoS, construction is inhomogeneous (the center of the image is darker than outside in (a)) (d), (e), and (f) are the jet-colored images of the gray scale (a), (b), and (c) respectively. (g), (h), and (i) are the pixel-value sums in vertical direction. Red arrows show the signal values outside the object regions. (h) and (i) have similar homogeneity characteristics; however, in (g), the middle region has smaller values. In (i), noise is less. As shown with arrow in (d), SoS is not homogeneous. MRI machine used prescan data for inhomogeneity correction; however, in (c) no additional acquisition data is used. Contrast and details are better in (c) than in (b) in all regions of the brain. In addition, there are artifacts outside the head, as shown with an arrow in (e), whereas (f) is much better.

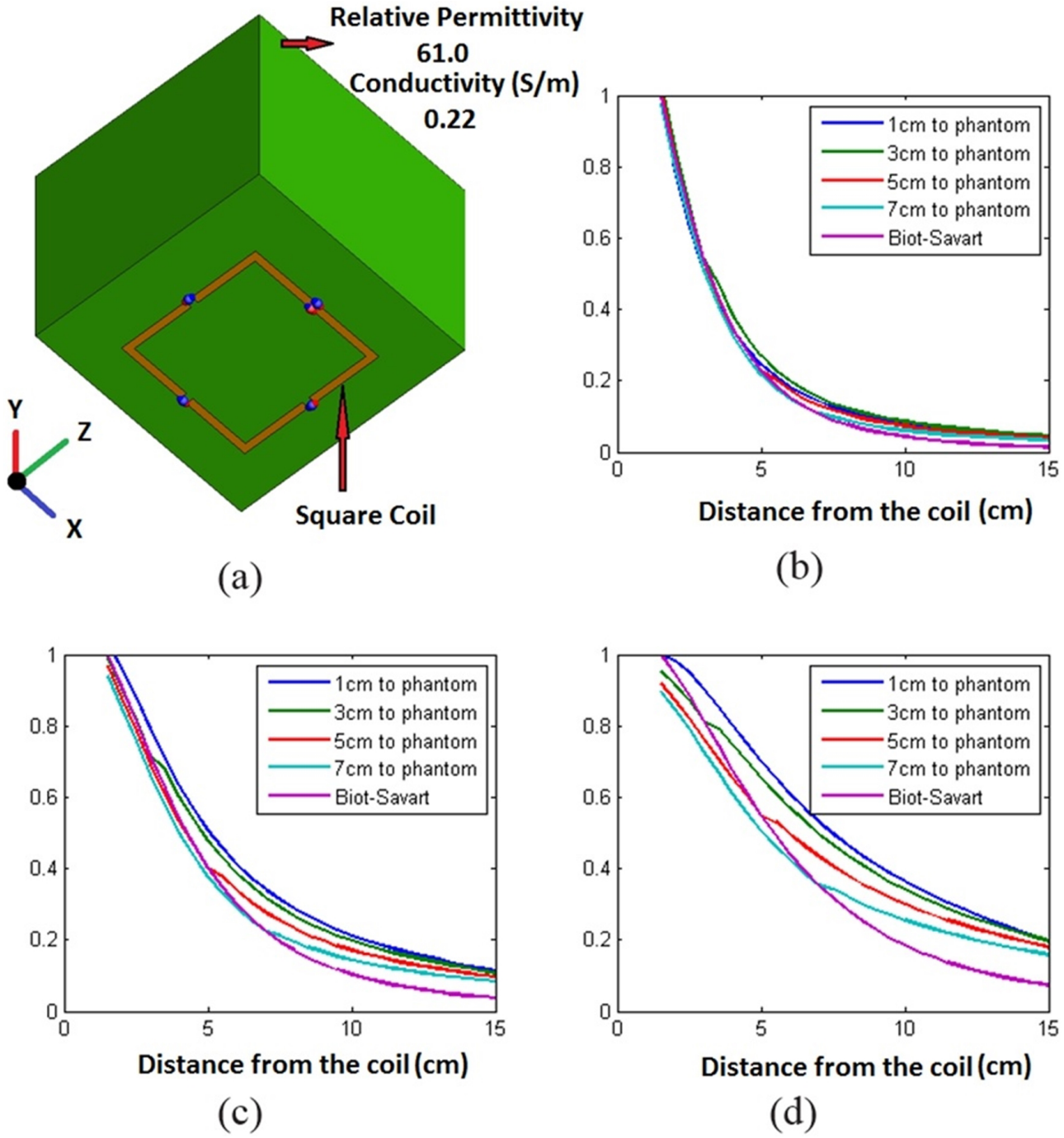

Figure 9. Simulation results for three different-sized square coils with a phantom. An illustration of the experimental setup, a comparison of the simulated B_1^- magnitudes, and the calculated BiotSavart ones are given. (a) 20 × 20 × 20 cm cube phantom and a square-shaped coil element; (b) normalized magnitude results of coil with a side length of 6 cm; (c) 9 cm; (d) 12 cm.

Table. Current percentage change through the coil conductor.

		Coil-to-phantom distance			
		1 cm	3 cm	5 cm	7 cm
Coil side length	6 cm	0.06502	0.00547	0.00563	0.00560
	9 cm	0.34713	0.00091	0.00113	0.00112
	12 cm	0.42	0.00523	0.00375	0.00368

method are consistent and satisfactory in each scenario. A group of experts (2 radiologists, a neurologist, 2 expert doctors, and 9 medical image-processing professionals) analyzed the results of more than 20 MRI images, and compared the outputs generated by the machine as well as those obtained by the proposed method. In addition, experiments on the simulation tool show that the success of the proposed method depends heavily on the size of the coil.

In the proposed method, one of the most important steps was to determine the exact coil element positions in 3D imaging space. Since the head coil is fixed to the patient table, its position, and, thus, the location of each coil element with respect to the image slices were calculated precisely. It was seen that in the case of a miscalculation, even with small errors (like several millimeters), the quality of the reconstructed images decreases.

As stated earlier, one of the main usage areas of MRI is to image the internals of the head. Fortunately, most of the head coils are fixed to the patient tables and are rigid. The exact coil shape can be obtained from the coil manufacturers. Using the coil shape and table position information, finding the location of each coil element relative to the image slice is a relatively easy task. The calculation of coil sensitivity magnitude maps is not a very time-consuming task; they can be computed once and used anytime. Therefore, coil sensitivity magnitude maps will be ready before an examination, and after a position adjustment operation they can be used directly. Thus, postprocessing duration will not be affected by the proposed method.

In [9], the Biot–Savart law was used in the enhancement of coil sensitivity maps on simulated data. In the study, a priori knowledge of approximate coil geometry was utilized, and the sensitivity of the coils was refined using optimization processes. However, as in our head coil case, in real life the geometry of the coil elements is not restricted to basic shapes. Therefore, it may not be possible to find the coil geometries from the raw sensitivity profiles, and the proposed method cannot guarantee good performances on complex coil shapes. Moreover, that method is applicable to low fields ($B_0 \leq 1.5$ T) and cannot be used in high ones. Furthermore, scanned object internals may cause unexpected consequences to such an approach.

With the advent of stronger magnets ($B_0 \geq 3$ T), RF field homogeneity becomes problematic. RF shimming can be used for transmit field homogeneity, but for receive field, coil sensitivities and body internals are important. The proposed method can be considered as an alternative method for inhomogeneity correction, because coil sensitivity information can also be used solely for correcting intensity variations on the images, as illustrated in Figure 8. In addition, according to our experts, the proposed method provided improved homogeneity (Figures 6 and 7).

As stated in [9], the known method for finding coil sensitivities is the division of the coil image with a known uniform reference image, which is obtained either from a body coil or the SoS of all coil channel elements. However, such methods suffer from two main problems. Firstly, in higher magnetic fields, neither the body coil image nor the SoS of surface coil images are uniform. Secondly, the division process causes additional errors, especially in low-proton density areas in the images [5], since the noise is augmented by division in

these regions. The proposed solution for sensitivity mapping does not carry any proton density information; therefore, the noise level does not increase. Moreover, in the division approach, the created sensitivity maps have lower resolution, since the reference images typically have lower resolution than the actual ones. Before using interpolation techniques in the reconstruction process, the resolution of the sensitivities is equalized to the actual images. This process creates additional errors and decreases the sharpness of the final image. However, in the proposed method, the resolution of the sensitivity maps is independent from the scan configuration, and higher resolution maps can be calculated easily.

In the proposed method, only the phase images of the reference low resolution signal data were used. Phase images are not affected as much as magnitude images by phase encoding line counts in reference scans. Therefore, the total scan can be accelerated by decreasing the phase-encoding lines in reference scans. Moreover, with further studies, phase images can be calculated without additional scans or prescan data. Thus, the examination time can be decreased. In such a case, since the sensitivity maps are computed, artifacts will be eliminated in sensitivity estimations due to usage of low-resolution reference data. Although the load (head or phantom) effect was taken into account in the phase values of sensitivity maps, it was ignored in magnitude values. When the results of the experiments are analyzed, our method is found to be successful in a 32-channel head coil. This means that the assumptions made in this study did not create a noticeable problem in reconstruction.

An earlier study by Ibrahim et al. [20] discussed the load effect on RF fields. This study showed that the dielectric media (tissue or phantom) alter the wave propagation, compared to air/free-space in high fields ($B_0 \geq 3$ T). This concurs with our simulation results, shown in Figure 9. However, according to our results, the difference between the actual magnitude values and the Biot–Savart law results becomes smaller as the coil size decreases. We also showed the effect of coil-to-phantom distance in Figures 9b–9d. It is seen that when the electromagnetic wave propagates from one medium (air) to another (phantom), the wave bends; however, the rate of decrease in magnitude does not change significantly between different mediums (tissues of the head) for small coils. In a recent study [21], a lossy, multilayered spherical head phantom was designed, which has similar radial conductivity and permeability profiles to the human head. RF field behavior in the human head was analyzed both with surface and volume coils. In the study, various coil sizes (6–10 cm radii) in different distances (0.5–4 cm) to the model were tested, and magnetic, electric field, specific absorption rate (SAR) pattern, and loss resistance were measured for each case. Our results are in accordance with this study; loss resistance increases with RF frequency and the radii of the coil, and decreases with coil–phantom distance.

Our method has not been tested for different coil geometries. We expect to see failure in coils with large coil elements. Similarly, when the tuning of the coil elements is poor, or if there is coupling between elements of the coil, the performance of the method will degrade. To understand the usefulness of the proposed method for calculating sensitivity maps, more testing should be carried out under different conditions.

We conducted a questionnaire for experts to compare the results obtained with the proposed method to the output generated by the machine in terms of image quality (resolution, sharpness, artifact level, and contrast). Fourteen experts preferred the results we obtained because they showed better resolution, sharpness, and a low level of artifact. Nine experts, including radiologists and a neurologist, found the quality increase significant. Six experts selected our method, as it provided improved contrast, and the other height reported that the contrast was similar in both methods. We calculated signal-to-noise ratio (SNR) values for all images,

and our method shows at least 11% better SNR for all cases.

$$SNR = \frac{\text{pixel value sum of the object region}}{\text{pixel value sum of the region outside of the object}}$$

We expected to obtain homogeneous images over the same tissue on phantom images. For this purpose, we tested the intensity changes over phantom images and compared the results with the machine's output. In accelerated scans, especially over the folded parts, intensity differences in the images are about 10% for the machine and 1% for our proposed method. In normal scans, the intensity difference between images over the object pixels is less than 3%. The machine promises homogeneity using prescan. Signal change over an image is given in Figures 8g–8i for comparison.

In short, our analysis and previous studies show that if the coil size is small and there is no other significant error source, the proposed method can be used for parallel image reconstruction and intensity correction in images. The proposed method has produced successful results using a 32-channel head coil. We think that further studies, where the usefulness of the proposed method will be tested in different settings and on other small coils available in the market, will improve our method and make it ready for use in practical life. In such a case, future coil designs will be influenced.

6. Conclusion

This study proposed a new method to calculate complex-valued coil sensitivities at 3 T. This method was applied to seven volunteers and a phantom in various setups, using a commercial 32-channel head coil. Moreover, the positive performance of the proposed approach was supported with simulations on electromagnetic simulation software. It was shown that, using this method, the images can be reconstructed with one of the known parallel imaging techniques (such as SENSE). According to the results of the experiments, our method generated more uniform images with better resolution and less artifacts compared to the sensitivity maps obtained using low-resolution full k-space data. This method increases image quality significantly, and can be used solely for intensity correction purposes without losing the diagnostic quality of the images.

Acknowledgments

We thank Prof Ergin Atalar. This work is supported by a TÜBİTAK PhD scholarship.

References

[1] Blaimer M, Breuer F, Mueller M, Griswold M A, Jakob P M. SMASH, SENSE, PILS, GRAPPA: how to choose the optimal method. Top Magn Reson Imag 2004; 15: 223-236.

[2] Pruessmann, KP, Weiger M, Scheidegger MB, Boesiger P. SENSE: sensitivity encoding for fast MRI. Magn Reson Med 1999; 42: 952-962.

[3] Griswold MA, Jakob PM, Wang J, Kiefer B, Haase A. Generalized autocalibrating partially parallel acquisitions (grappa). Magn Reson Med 2002; 47: 1202-1210.

[4] Heidemann RM, Özsarlak Ö, Parizel PM, Michiels J, Kiefer B, Jellus V, Müller M, Breuer F, Blaimer M, Griswold MA et al. A brief review of parallel magnetic resonance imaging. Eur Radiol 2003; 13: 2323-2337.

[5] Griswold MA, Breuer F, Nittka M, Jellus V, Kiefer B, Jakob PM. Autocalibrated coil sensitivity estimation for parallel imaging. NMR Biomed 2006; 19: 316-324.

[6] Bradley WG, Brant-Zawadski M, Cambray-Forker J. MRI of the Brain. Vol. 1. Philadelphia, PA, USA: Lippincott Williams & Wilkins, 2001.

[7] Baert AL, Prayer D. Fetal MRI. Berlin, Germany: Springer, 2011.

[8] Pruessmann KP. Encoding and reconstruction in parallel MRI. NMR Biomed 2006; 19: 288-299.

[9] Jin J, Liu F, Crozier S. An electromagnetic reverse method of coil sensitivity mapping for parallel MRI—theoretical framework, J Magn Reson 2010; 207: 59-68.

[10] Hoult D. The principle of reciprocity in signal strength calculations—a mathematical guide. Concept Magnetic Res 2000; 12: 173-187.

[11] Wiesinger F, de Moortele V, Adriany G, Ugurbil K, Pruessmann KP. Potential and feasibility of parallel MRI at high field. NMR Biomed 2006; 19: 368-378.

[12] Poston A. Human Engineering Design Data Digest: Human Factors Standardization Systems. Washington, DC, USA: Federal Aviation Administration, 2000.

[13] Gabriel S, Lau R, Gabriel C. The dielectric properties of biological tissues: III. Parametric models for the dielectric spectrum of tissues. Phys Med Biol 1996; 41: 2271-2293.

[14] Cherry SR, Badawi RD, Qi J. Essentials of In Vivo Biomedical Imaging. Boca Raton, FL, USA: CRC Press, 2015.

[15] Lerner LS. Physics for Scientists and Engineers. Burlington, MA, USA: Jones & Bartlett Learning, 1997.

[16] Bankson JA, Wright SM. Simulation-based investigation of partially parallel imaging with a linear array at high accelerations. Magn Reson Med 2002; 47: 777-786.

[17] Kamel IR, Elmar MM. Body MR Imaging at 3 Tesla. Cambridge, UK: Cambridge University Press, 2011.

[18] Wang J, Kluge T, Nittka M, Jellus V, Kiefer B. Parallel acquisition techniques with modified SENSE reconstruction (mSENSE). In: Proceedings of the First Würzburg Workshop on Parallel Imaging Basics and Clinical Applications; 2001; Würzburg, Germany. p. 89.

[19] Zhang Y, Peterson BS, Dong Z, A support-based reconstruction for SENSE MRI. Sensors 2013; 13: 4029-4040.

[20] Ibrahim TS, Mitchell C, Schmalbrock P, Lee R, Chakeres DW. Electromagnetic perspective on the operation of RF coils at 1.5–11.7 Tesla. Magn Reson Med 2005; 54: 683-690.

[21] Xu B, Li BK, Crozier S, Liu F. Model implementation and case study for the lossy, multilayered spherical head phantom in MRI application. In: IEEE–EMBS 2005 Engineering in Medicine and Biology Society Conference; 1–4 September 2005; Shanghai, China. New York, NY, USA: IEEE. pp. 1400-1403.